Int. J. Electrochem. Sci., 10 **(2015)** 7361 - 7370

International Journal of
ELECTROCHEMICAL
SCIENCE
www.electrochemsci.org

Graphene-Wrapped Cr_2O_3 Hollow Nanospheres with Enhanced Electrochemical Performances for Lithium-Ion Batteries

Hui Xu, Min Zeng[*]*, Jing Li*

School of Materials Science and Engineering, Southwest University of Science and Technology, Mianyang 621010, P R China
[*]E-mail: zengmin@swust.edu.cn

Received: 2 June 2015 / *Accepted:* 7 July 2015 / *Published:* 28 July 2015

Graphene-wrapped Cr_2O_3 hollow nanospheres were prepared using a facile two-step process by solvothermal to synthesize Cr_2O_3 hollow nanospheres and then hydrothermal reduction of the GO with urea to yield graphene coating on Cr_2O_3 hollow nanospheres. The graphene/Cr_2O_3 composites exhibit not only a high reversible capacity of over 700 $mAhg^{-1}$ for the first cycle, but also an outstanding cycling stability and rate capability. Various characterization methods indicate that the Cr_2O_3 hollow nanospheres are uniformly distributed on the surface and interlayer of graphene sheets. The positive synergistic effect of the Cr_2O_3 hollow nanospheres and graphene coating may be beneficial to improve electrochemical performances of these composite electrodes.

Keywords: lithium-ion batteries, graphene, Cr_2O_3 hollow nanospheres, synergistic effect

1. INTRODUCTION

Energy storage has become one of the great challenges in the 21st century. Lithium-ion batteries (LIBs), as an effective energy storage device, have been intensively pursued and widely used as power sources for portable devices (e.g. mobile phones) due to their outstanding superiorities such as low self-discharge, long cycle life, high energy density, no memory effect, environmental friendliness and light weight [1,2]. In recent years, electric vehicles have been considered to be the most promising candidate to replace traditional vehicles, and the rapid development of vehicle electrification not only provides good prospects for the applications of LIBs, but also puts forward higher requires on the performances of LIBs [3]. Graphite has been widely employed as a conventional anode material of LIBs due to its low cost and good cycling stability, however, relatively low theoretical capacity (370 $mAhg^{-1}$) and poor rate capability have become an obstacle for graphite as a power battery anode material in the future. In order to meet the increasing requirements for upcoming

vehicle electrification, it is essential to develop new high-performance electrode materials for LIBs [4]. Transition metal oxides (Cr_2O_3 [5-7], MnO_2 [8], Fe_2O_3 [9], Co_3O_4 [10]) have been exploited as the anode materials of LIBs due to their substantial superiorities [11], such as intrinsically enhanced safety, high lithium storage capacity and widespread availability. However, their intrinsically induced drastic volume expansion/contraction and low electrical conductivity lead to electrode pulverization and loss of charge transfer, resulting in a rapid capacity decay and poor cycling performance [12]. To circumvent these obstacles, a variety of strategies have been devoted to alleviating the volume change and improving the electrical conductivity, such as nanoscale materials [13] and mesoporous structure materials [14], especially with hollow structure materials [6] and carbon-based composites [7] usually have good electrochemical performances.

Graphene has attracted extensive interest in the last decade due to its outstanding strengths including ultralarge specific surface area, good conductivity and excellent flexibility [15]. Herein, multifarious graphene-based transition metal oxides are emerging as a new kind of composites that are considered to be promising for many applications (e.g. LIBs or supercapacitor) [16-18]. In this manuscript, we report a facile strategy to synthesize graphene-wrapped Cr_2O_3 hollow nanospheres as a high-performance anode material for LIBs. As a special structure of carbon with many excellent properties, graphene seems to be an ideal substrate material for Cr_2O_3 to improve its cycling performance and electrical conductivity. Electrochemical investigations display that the composites possess a high reversible capacity, outstanding cycling performance and good rate capability.

2. EXPERIMENTAL

2.1. Preparation of graphene oxide

Graphene oxide (GO) was synthesized from graphite flakes by an improved Hummer's method [19]. In brief, 2 g of $NaNO_3$ and 2 g of graphite were added into 90 mL of 98% H_2SO_4 under stirring in an ice bath. 12 g of $KMnO_4$ was introduced slowly in portions to the mixture under vigorous stirring for about an hour. The reaction was transferred to 35 °C and then stirred for about 30 min. Subsequently, the reaction was again placed in an ice bath and 180 mL of ultrapure water was dropwise added into the mixture. 560 mL of ultrapure water and 10 mL of 30 % H_2O_2 were poured into the mixture after the mixture was stirred at 98 °C for about 20 min. Meanwhile, a large number of bubbles emerged in solution and the color of the mixture turned from brown to yellow. The product was washed with ultrapure water until the pH was close to neutral. Finally, as-prepared GO was dispersed in ultrapure water (0.5 mg/mL) under ultrasonication for 5 h to form a homogeneous suspension.

2.2. Preparation of graphene/ Cr_2O_3 composites

Cr_2O_3 hollow nanospheres (denoted as bare Cr_2O_3) were prepared prior according to the similar method by Jiang [6]. Graphene-wrapped Cr_2O_3 hollow nanospheres (denoted as graphene/Cr_2O_3) were prepared by a hydrothermal method, as schematically shown in Figure 1.

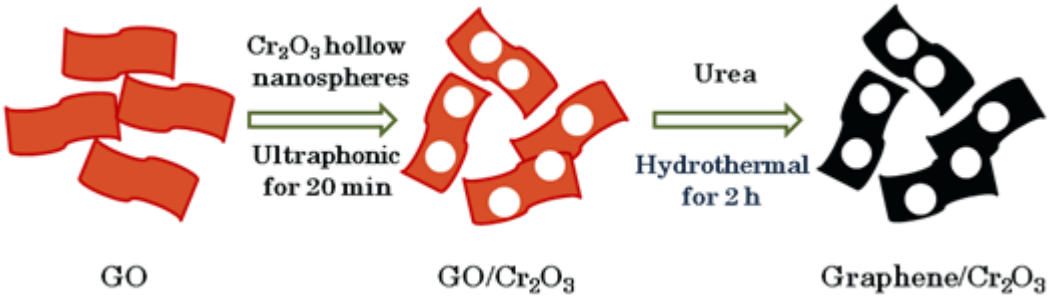

Figure 1. Schematic representation of the preparation process of graphene/Cr_2O_3 composites.

In brief, 0.05 g as-prepared Cr_2O_3 hollow nanospheres were dispersed into 80 mL of GO dispersion (0.5 mg/mL) under ultrasonication for 20 min, followed by stirring for 1 h. 0.1 g of urea was introduced into the suspension with stirring for another 1 h. The reaction was transferred to a 100 mL Teflon-lined autoclave, then sealed and heated at 120 °C for 2 h. The resulting black precipitate was filtered using a fat-soluble membrane, washed thoroughly with ultrapure water and then dried at 60 °C for 12 h under vacuum.

2.3. Materials Characterizations

The samples were initially characterised by X-ray diffraction using an X-ray diffraction analyzer with Cu-Kα radiation (X´Pert PRO, PANalytical). Raman tests were carried out using a Renishaw Invia with a laser wavelength of 514.5 nm. The morphology and composition of as-prepared graphene/Cr_2O_3 composites were examined using field emission scanning electron microscope (Ultr55, Zeiss) equipped with energy dispersive X-ray spectrometer (EDX). The thermogravimetric (TG) analysis and differential scanning calorimetry (DSC) analyses were examined from the SDT Q600 thermal analyzer with a heating rate of 10 °C·min^{-1} over the range 30 °C -800 °C in an air atmosphere.

2.4. Electrochemical Characterization

The electrochemical performances were evaluated using CR2016-type coin cell. The working electrodes were fabricated by mixing the active materials, super P and polyvinylidene difluoride (PVDF) in a weight ratio of 8:1:1, and then milled homogeneously in an agate mortar. Subsequently, an appropriate amount of N-methylpyrrolidone (NMP) solvent was slowly introduced and wet mixed to produce electrode slurry. The uniform slurry was coated onto a copper foil using a scraper and dried at 120 °C for 24 h. Then the electrodes were punched into disks and assembled into half cells in an Ar-filled glove box. Li foils were used as the counter electrodes and the polypropylene microporous films (Celgard 2300) were employed as the separators. The commercial electrolyte was 1 M solution of $LiPF_6$ in dimethyl carbonate (DMC) and ethylene carbonate (EC) with in a volume ratio of 1:1. The galvanostatic charge-discharge tests were carried out using a LAND test system in the voltage range of 0.01 to 3.0 V (vs. Li/Li$^+$). Electrochemical impedance spectroscopy (EIS) was tested using a CHI760C

electrochemical station in the frequency range of 0.005 to 100000 Hz with a potentiostatic signal amplitude of 5 mV.

3. RESULTS AND DISCUSSION

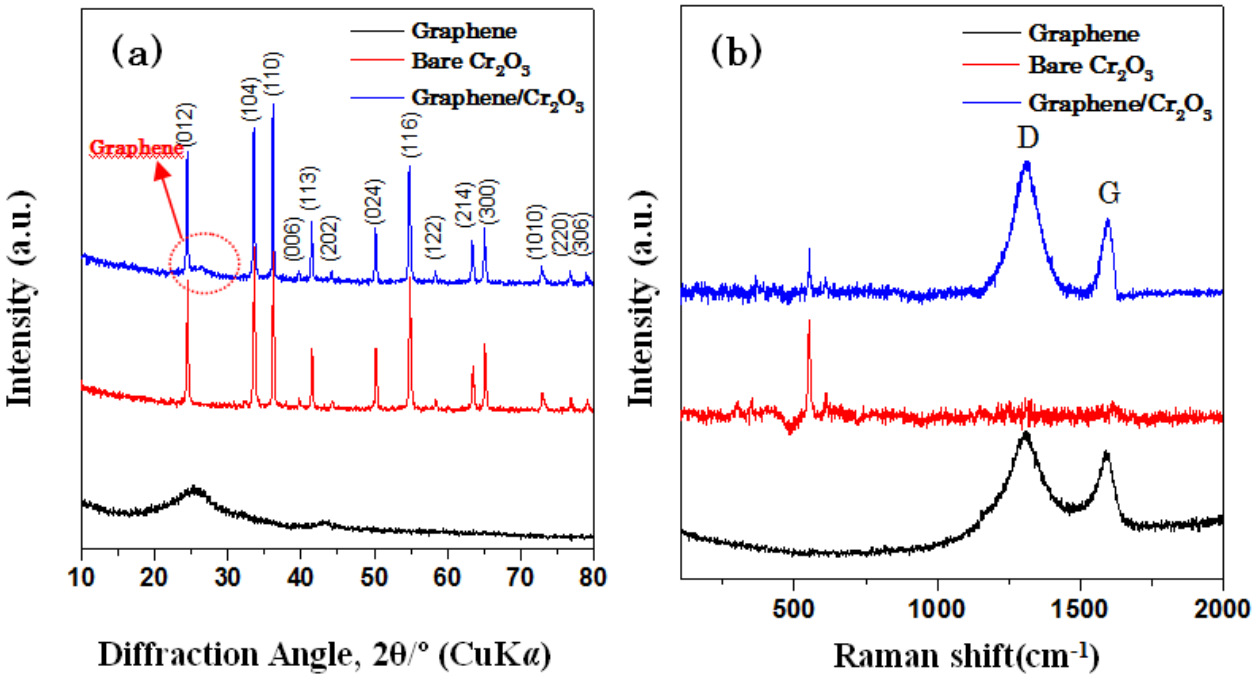

Figure 2. (a) XRD patterns and (b) Raman spectra of graphene, bare Cr_2O_3 and graphene/Cr_2O_3 composites.

The X-ray diffraction patterns of graphene, bare Cr_2O_3 and graphene/Cr_2O_3 composites are shown in Figure 2 (a). The pattern of graphene shows a broad (002) diffraction peak at 2θ of 26°, which can be regarded as the stacked graphene sheets [20]. The characteristic diffraction peaks of bare Cr_2O_3 and graphene/Cr_2O_3 composites correspond to the (012), (104), (110), (006), (113), (202), (024), (116), (122), (214), (300), (1010), (220) and (306) planes of well-crystallized rhombohedral Cr_2O_3 (space group R-3c, a = 0.4957 nm, b = 0.4957 nm and c = 1.3592 nm). Compared with those bare Cr_2O_3, an additional stacking peak appears at 26° in graphene/Cr_2O_3 composites pattern, suggesting that GO was possibly reduced to graphene in composites. It's worth noting that the stacking peak of graphene/Cr_2O_3 composites is very weak, indicating the formation of more disordered graphene sheets in graphene/Cr_2O_3 composites. Moreover, there are any no impurity peaks are detected in the XRD results of graphene/Cr_2O_3 composites, indicating the formation of high purity product.

Further information about the structure of the graphene sheets in the graphene/Cr_2O_3 composites can be acquired with Raman spectra. Raman spectra of graphene, bare Cr_2O_3 and graphene/Cr_2O_3 composites are shown in Figure 2 (b). The peaks located at about 550 cm^{-1} are detected in bare Cr_2O_3 and graphene/Cr_2O_3 composites, which can be attributed to Cr-O lattice

vibrations [21]. The conventional D and G band peaks at 1315 and 1595 cm^{-1} can be observed in graphene and graphene/Cr_2O_3 composites, indicating the existence of graphene sheets in composites [22]. I_D/I_G of D and G bands peaks of the composites is about 1.8, much higher than those of other graphene-based materials reported in elsewhere [22], implying the more disordered structure result from graphene [23]. The above results are consistent with the results of XRD.

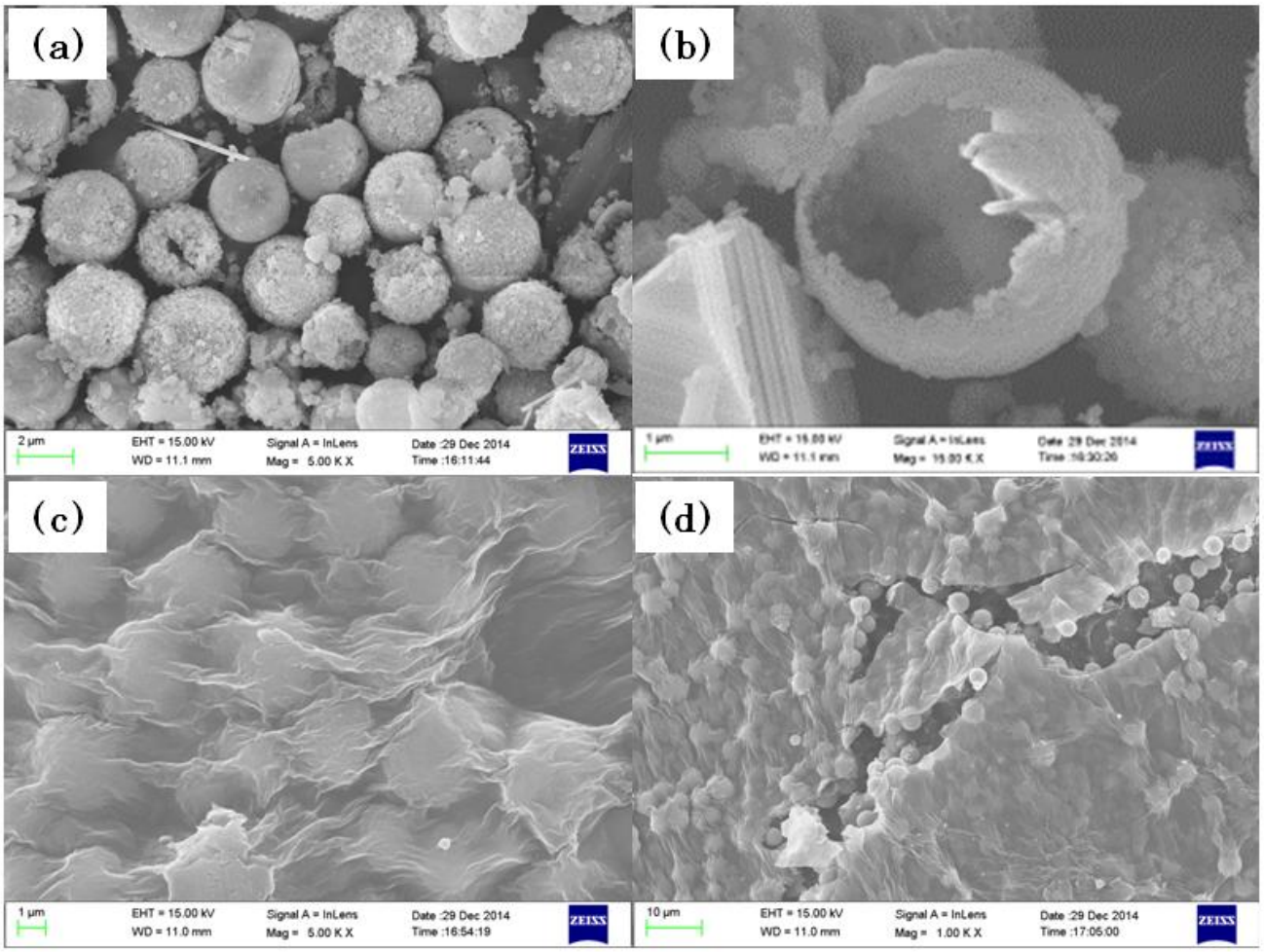

Figure 3. FESEM images of bare Cr_2O_3 and graphene/Cr_2O_3 composites..

The morphology and structure of bare Cr_2O_3 and graphene/Cr_2O_3 composites are illustrated by field emission scanning electron microscopy (FESEM). It can be seen from Figure 3 (a) that the bare Cr_2O_3 exhibits a uniform diameter of about 2 μm, and an obvious hollow structure can be observed in Figure 3 (b). Figure 3 (c) shows a paperlike graphene coating, constituting a thin curled "wrinkle-like" morphology, is closely wrapped the surface of the Cr_2O_3 hollow nanospheres. The nanospheres distribute homogeneously on the surface and interlayer of graphene sheets. The graphene/Cr_2O_3 composites present layer-by-layer stacking structure, these hierarchical constructions can be seen clearly in Figure 3 (d). To verify the structure and composition of graphene/Cr_2O_3 composites, we

carried out energy dispersive X-ray spectroscopic mapping of our material. As shown in Figure 4, we can recognize that O, Cr and C are uniformly distributed in the composites.

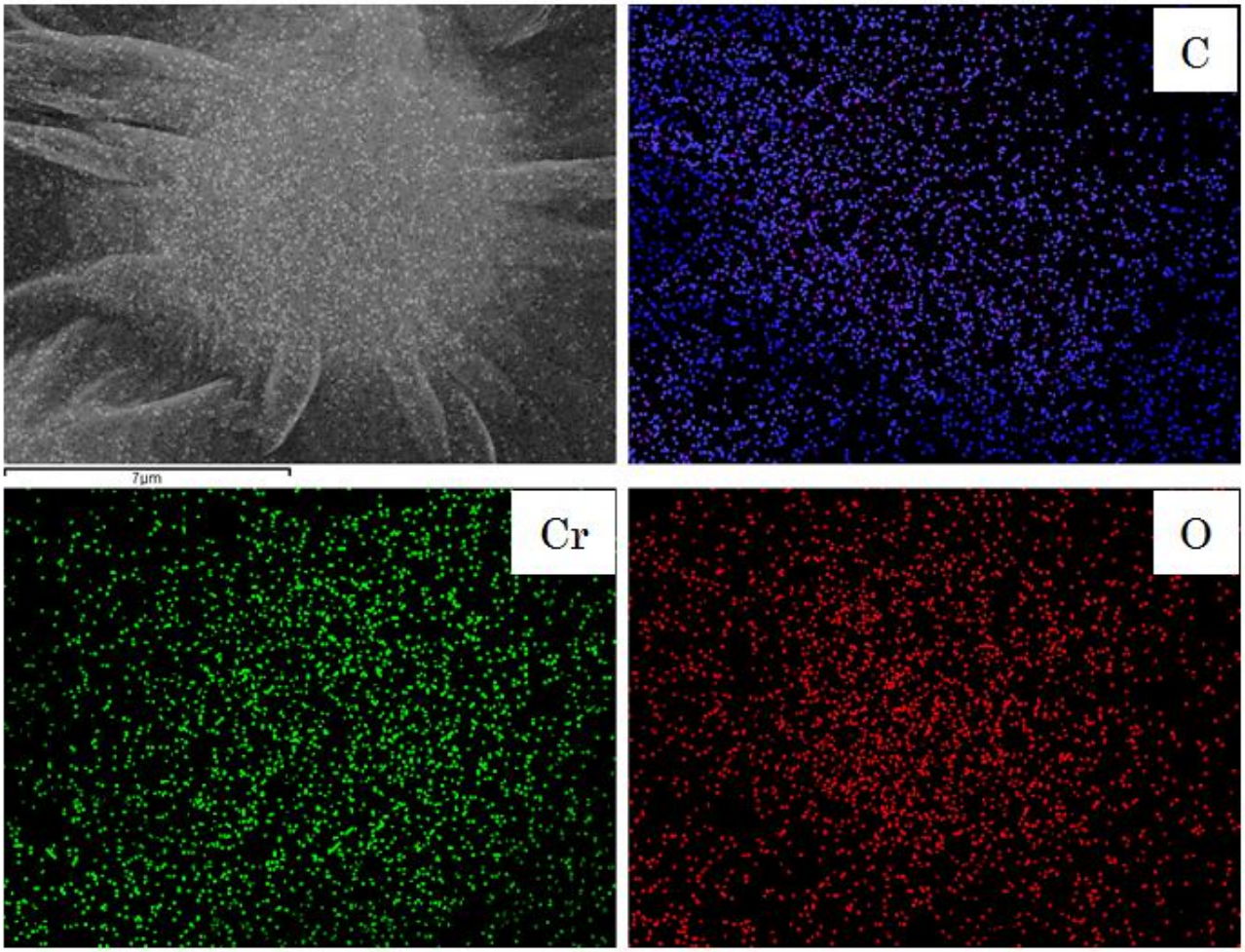

Figure 4. SEM image and the corresponding elemental mapping of O, Cr and C in the graphene/Cr_2O_3 composites.

Thermogravimetric (TG) analysis and differential scanning calorimetry (DSC) analyses of graphene/Cr_2O_3 composites were performed from room temperature to 800 °C in air. As shown in Figure 5, the TG curve illustrates a loss of 1.65% from the room temperature to around 100 °C, which could be attributed to the release of physically adsorbed water. When the temperature is increased from 100 °C to 600 °C, the mass loss is as high as 16.3%, the accompanying an intense exothermic peak in the DSC curve could be attributed to the combustion of the graphene. The results of thermoanalysis indicate that the graphene content in the graphene/Cr_2O_3 composites is evaluated to be about 16.3%.

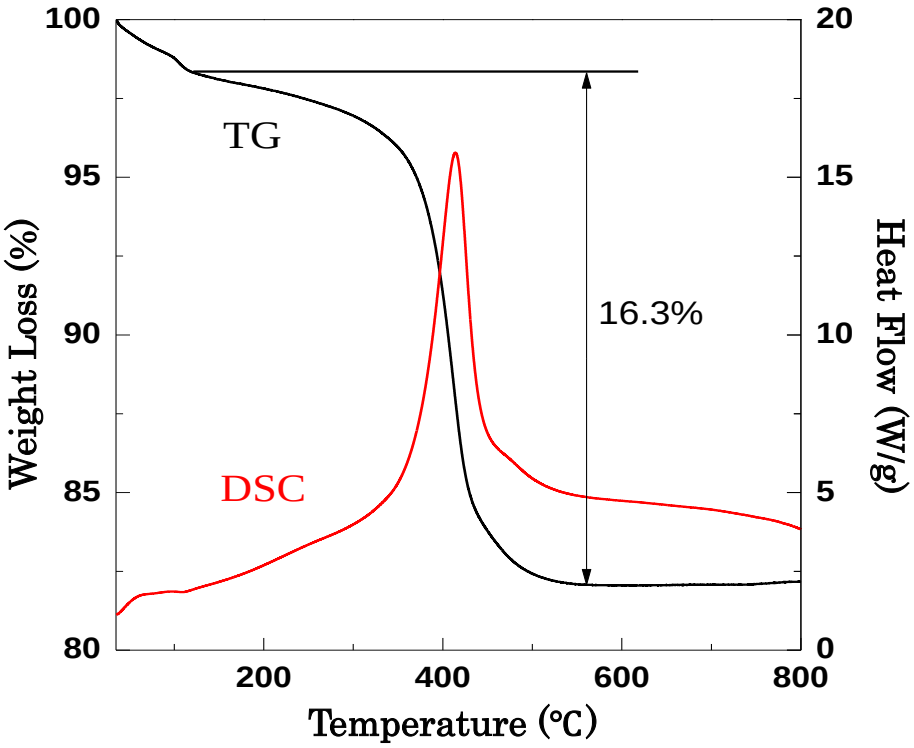

Figure 5. TG-DSC traces of the graphene/Cr_2O_3 composites.

The lithium storage performance of graphene/Cr_2O_3 composites was initially investigated by galvanostatic measurements at a rate of 0.1C. Figure 6 (a) shows the discharge/charge curves of graphene/Cr_2O_3 composites in the 1st, 2th, 5th, and 10th cycles. Only one plateau in the discharge process corresponds to the following transformation reaction:

$Cr_2O_3 + 6Li^+ \leftrightarrow 2Cr^{3+} + 3Li_2O$

which is consistent with the lithium storage mechanism of other Cr_2O_3-based anodes [6,7]. The first discharge and charge capacities of graphene/Cr_2O_3 composites are 1460 and 702 $mAhg^{-1}$, the first coulombic efficiency of graphene/Cr_2O_3 composites is only about 48% and the initial large capacity loss may result from the incomplete conversion reaction and irreversible lithium loss because of the formation of an unstable solid electrolyte interphase (SEI) film [20,24].

However, the coulombic efficiency soars from 48% in the first cycle to 87% in the second cycle, 94.5 in the fifth cycle, 96.9% in the tenth cycle and then remains above 97% in the subsequent cycles. The cycling performance of graphene/Cr_2O_3 composites is illustrated in Figure 6 (b). For comparison, we also show the results of graphene and bare Cr_2O_3. The graphene/Cr_2O_3 composites present the best cycling performance. After 100 discharge/charge cycles, the reversible capacity still maintains more than 580 $mAhg^{-1}$, while graphene and bare Cr_2O_3 can only deliver a lower reversible capacity of 337 $mAhg^{-1}$ and 312 $mAhg^{-1}$, respectively.

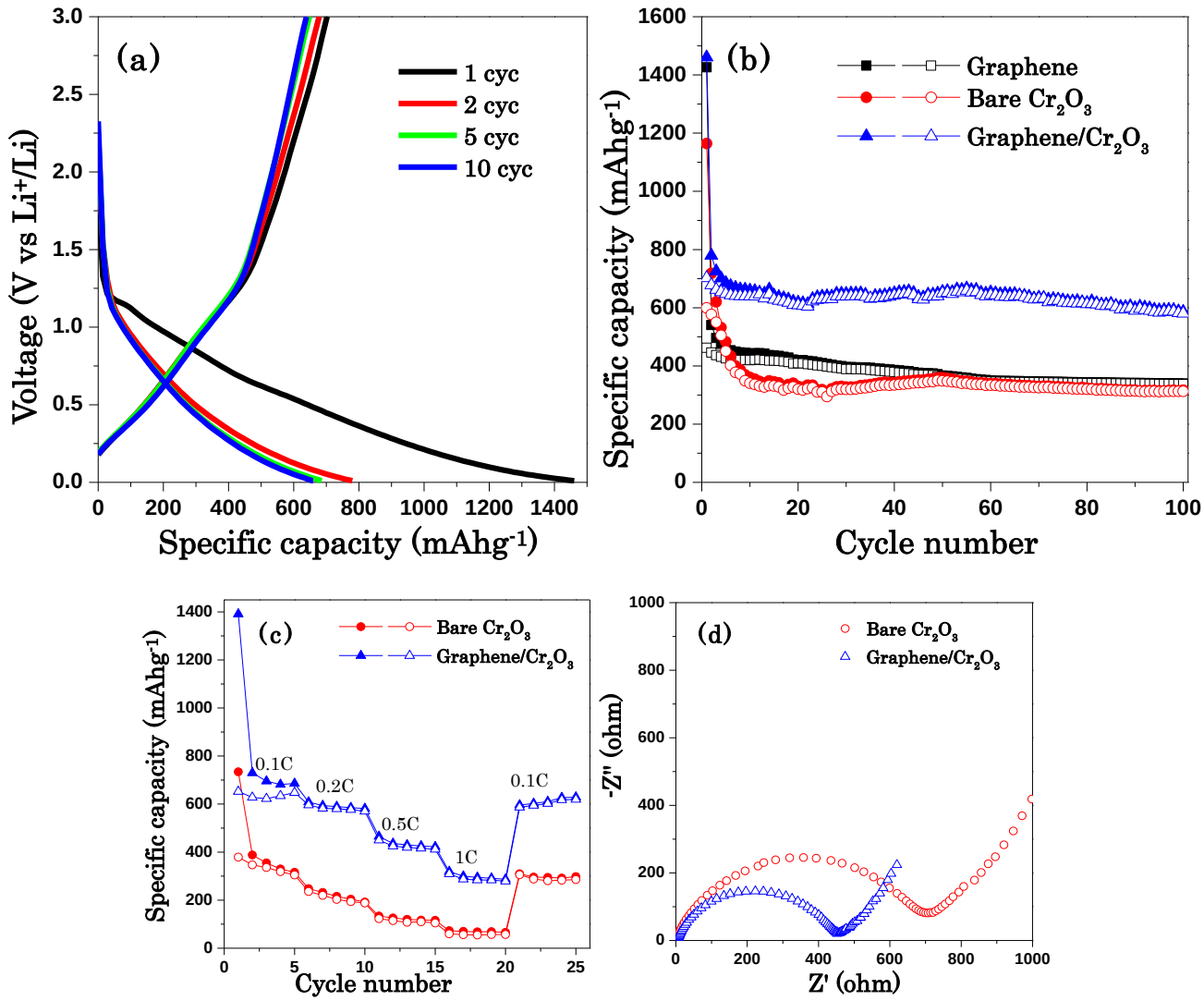

Figure 6. (a) Galvanostatic charge-discharge curves of graphene/Cr_2O_3 composites, (b) cycling performance of graphene, bare Cr_2O_3 and graphene/Cr_2O_3 composites, (c) rate capability and (d) electrochemical impedance spectra of bare Cr_2O_3 and graphene/Cr_2O_3 composites.

It can be found that the combination of the flexible graphene and the hollow nanospheres may make a greater contribution to the cycling performance than that of single graphene or hollow nanospheres. In addition, the capacity retention of graphene/Cr_2O_3 composites reaches up to 82.6% after 100 cycles, which is also higher than graphene (72.9%) and bare Cr_2O_3 (78.2%). The prominent cycling performance of graphene/Cr_2O_3 composites is not only ascribed to the characteristic hollow nanostructure which contributes to faster diffusion of electrolyte [6], but also the high electrical conductivity and the large electrochemical active surface area of graphene which are favourable for the transport and storage of lithium ions [20]. Figure 6 (c) shows the rate capability of graphene/Cr_2O_3 composites and bare Cr_2O_3 operated at various rates of 0.1C to 1C. Graphene/Cr_2O_3 composites exhibit much better rate capability compared to the bare Cr_2O_3, even at a high rate of 1 C, which is still as high as 284 $mAhg^{-1}$. Besides, the capacity of 619 $mAhg^{-1}$ is retained after 25 cycles when the current density recovers to 0.1 C, also suggesting its good rate capability. However, the capacity of the bare

Cr_2O_3 decreases dramatically at higher rate, a lower capacity of 55 $mAhg^{-1}$ is obtained at 1 C. These results strongly demonstrate that the graphene coating and the layer-by-layer structure play a crucial role in improving the cycling stability and rate capability. The flexible graphene coating acts as a "bridge" between these Cr_2O_3 nanospheres, which is favorable for lithium ion rapid transport. In order to gain insight into the effect of the graphene coating, electrochemical impedance spectroscopy (EIS) tests were implemented. As shown in Figure 6 (d), the semicircle diameters of graphene/Cr_2O_3 composites are smaller than the bare Cr_2O_3, indicating a smaller charge-transfer resistance, as well as the contact resistance and SEI resistance attributed to the excellent conductivity of graphene. All the results demonstrate that graphene coating is beneficial to improve the discharge/charge performance of Cr_2O_3, making a reversible lithiation/delithiation reaction between Cr_2O_3 and Li.

The improved cycling performance of graphene/Cr_2O_3 composites can be assigned to the positive synergistic effect of the graphene and Cr_2O_3 [9,20]. The graphene coating on Cr_2O_3 hollow nanospheres may contribute to enhancing the structure stability, thus preventing them from pulverization, while also affording electrical conductivity to each sphere. It is especially important for insulating transition metal oxides in which significant phase transition and drastic volume expansion/contraction may occur during the cycle process. In contrast, without the graphene coating, the reversible capacity of bare Cr_2O_3 decreases from 599 to 312 $mAhg^{-1}$ after 100 cycles. As expected, the graphene coating effectively buffers the strain from the volume expansion/contraction of Cr_2O_3, resulting in the improvement of cycling performance of graphene/Cr_2O_3 composites.

The high reversible capacity, outstanding cycling performance and good rate capability make our graphene/Cr_2O_3 composites a promising potential anode material of LIBs. The excellent electrochemical performance of the graphene/Cr_2O_3 composites can be summarized as follows: (i) Graphene coating has an excellent conductivity [25] and acts as the conductive bridges between Cr_2O_3 nanospheres, which can reduce the inner resistance of the battery and is helpful for improving the electronic and ionic conductivity. Hence graphene/Cr_2O_3 composites have shown a higher specific capacity than that of bare materials. (ii) Graphene sheets not only alleviate the volume change of Cr_2O_3, but also efficiently provide active sites for Li insertion/desertion during the charge/discharge process, therefore leading to superior cycling performance and large capacity [26]. (iii) The large surface area of ultrathin graphene sheets and hollow nanostructure electrodes are beneficial to enlarge the electrode/electrolyte contact area, shorten the path length for Li transport [27]. (iv) Cr_2O_3 nanospheres distribute homogeneously in the interlayer of graphene, which can reduce the agglomeration of graphene sheets. According to the above discussions, we strongly convince that the synergy effect and intimate interaction between Cr_2O_3 and graphene are responsible for enhanced the electrochemical performance of composites.

4. CONCLUSION

In summary, we report a facile two-step process to synthesize graphene/Cr_2O_3 composites as a high-performance anode material for LIBs. This novel structure effectively improves the reversible capacity and the cycling performance of Cr_2O_3 based anode materials. The composites exhibit a high

reversible capacity (702 $mAhg^{-1}$) for the first cycle and a good capacity retention (580 $mAhg^{-1}$) after 100 cycle, which is much higher than that of graphene and bare Cr_2O_3 electrode materials. It is concluded that a positive synergetic effect of graphene and Cr_2O_3 is essential to enhance the electrochemical performance of the electrodes.

References

1. M. Armand and J. M. Tarascon, *Nature*, 451 (2008) 652.
2. J. M. Tarascon and M. Armand, *Nature*, 414 (2001) 359.
3. J. H. Kim, N. P. W. Pieczonka and L. Yang, *ChemPhysChem*, 15 (2014) 1940.
4. H. Li, Z. X. Wang, L. Q. Chen and X. J. Huang, *Adv. Mater*, 21 (2009) 4593.
5. J. Hu, H. Li and X. J. Huang, *Electrochem. Solid-State Lett.*, 8 (2005) A66.
6. L. Y. Jiang, S. Xin, X. L. Wu, H. Li, Y. G. Guo and L. J. Wan, *J. Mater. Chem.*, 20 (2010) 7565.
7. W. B. Yue, S. S. Tao, J. M. Fu, Z. Q. Gao, Y. Ren, *Carbon*, 65 (2013) 97.
8. A. P. Yu, H. W. Park, A. Davies, D. C Higgins, Z. W. Chen and X. C. Xiao, *J. Phys. Chem. Lett.*, 2 (2011) 1855.
9. X. J. Zhu, Y. W. Zhu, S. Murali, D. C Higgins, Z. W. Chen and X. C. Xiao, *ACS Nano*, 5 (2011) 3333.
10. X. Wang, X. L. Wu, Y. G. Guo, Y. T. Zhong, X. Q. Cao, Y. Ma and J. N. Yao, *Adv. Funct. Mater*. 20 (2010) 1680.
11. P. Poizot, S. Laruelle, S. Grugeon, L. Dupont and J. M. Tarascon, *Nature*, 407 (2000) 496.
12. J. P. Sun, K. Tang, X. Q. Yu, J. Hu, H. Li, X. J. Huang, *Solid State Ionics*, 179 (2008) 2390.
13. P. G. Bruce, B. Scrosati and J. M. Tarascon, *Angew*, *Chem. Int. Ed*, 47 (2008) 2930.
14. H. Liu, X. W. Du, X. R. Xing, G. X. Wang and S. Z. Qiao, *Chem. Commun.*, 48 (2012) 865.
15. A.K. Geim and K.S. Novoselov, *Nat. Mater.*, 6 (2007) 183.
16. X. D. Huang, B. Sun, S. Q. Chen and G. X. Wang, *Chem. Asian J.*, 9 (2014) 206.
17. J. S. Luo, J. L. Liu, Z. Y. Zeng, C. F. Ng, L. J. Ma, H. Zhang, J. Y. Lin, C. F. Ng, L. J. Ma, H. Zhang, J. Y. Lin, *Nano Lett.*, 13 (2013) 6136.
18. J. W. Lee, A. S. Hall, J. D. Kim and T. E. Mallouk, *Chem. Mater.*, 24 (2012) 1158.
19. D. C. Marcano, D. V. Kosynkin, J. M. Berlin, A. Sinitskii, Z. Z. Sun, A. Slesarev, L. B. Alemany, W. Lu and J. M. Tour, *ACS Nano*, 4 (2010) 4806.
20. Z. S. Wu, W. C. Ren, L. Wen, L. B. Gao, J. P. Zhao, Z. P. Chen, G. M. Zhou, F. Li and H. M. Cheng, *ACS Nano*, 4 (2010) 3187.
21. S. Khamlich, E. Manikandan, B. D. Ngom, J. Sithole, O. Nemraoui, I. Zorkani, R. McCrindle, N. Cingo, M. Maaza, *J. Phys. Chem. Solids*, 72 (2011) 714.
22. W. F. Chen, L. F. Yan, P. R. Bangal, *Carbon*, 48 (2010) 1146.
23. Z. J. Fan, J. Yan, G. Q. Ning, T. Wei, L. J. Zhi, F. Wei, *Carbon*, 60 (2013) 558.
24. J. Lin, Z. W. Peng, C. S. Xiang, G. D. Ruan, Z. Yan, D. Natelson, J. M. Tour, *ACS Nano*, 7 (2013) 6001.
25. Y. Q. Sun, Q. Wu and G. Q. Shi, *Energy Environ.*, 4 (2011) 1113.
26. G. Q. Ning, Z. J. Fan, G. Wang, J. S. Gao, W. Z. Qian and F. Wei, *Chem. Commun.*, 47 (2011) 5976.
27. J. S. Chen, Z. Y. Wang, X. C. Dong, P. Chen and X. W. (David) Lou, *Nanoscale*, 3 (2011) 2158.